

Benchmark of estimated solar irradiance data at high latitude locations

Heine Nygard Riise ^{a,*}, Magnus Moe Nygård ^a, Bjørn Lupton Aarseth ^a, Andreas Dobler ^b, Erik Berge ^b

^a Institute for Energy Technology, Department of Solar Power Systems, NO-2007 Kjeller, Norway

^b Norwegian Meteorological Institute, NO-0371 Oslo, Norway



ARTICLE INFO

Keywords:

Irradiance estimation
Benchmark
Global horizontal irradiance
Satellite-based irradiance estimates
Atmospheric reanalysis
Pyranometers

ABSTRACT

Estimated solar irradiances from CAMS, PVGIS SARAH-2, Solargis, Meteonorm, PVGIS ERA5, and NASA POWER are benchmarked against measurements conducted at 34 ground stations in Norway at latitudes between 58 and 76°N. We find that the data products that mainly rely on high-resolution, geostationary satellite images, i.e., CAMS, PVGIS SARAH-2, and Solargis, have higher accuracy with lower relative Mean Absolute Error (rMAE) and relative Mean Bias Error. By dividing the stations in distinct categories, such as above 65°N, snow-affected and horizon-shaded, challenges with irradiance estimation that are common in Norway and at high latitudes in general are highlighted and discussed. The accuracy of the data products is dependent on latitude, and by excluding stations above 65°N, the median rMAE of the different data products improves 3.2–9.4 %_{abs} compared to the median rMAE when including all stations, depending on data product. Similarly, by excluding snow-affected stations, the median rMAE improves 1.9–8.1 %_{abs}, depending on data product. The improvement in rMAE by excluding snow-affected stations is partially related to the difficulty of separating snow on the ground from cloud cover in satellite images. This difficulty is illustrated by concrete examples of irradiance time series from clear sky days when the ground is covered in snow. Although the performance of the data products is dependent on the categorization of stations, i.e., latitude, snow conditions, and local topography, the relative performance between the products is maintained regardless of sub-division.

1. Introduction

Solar irradiance data is important in several different fields, in disciplines as varied as energy, architecture, climatology, and agriculture. It is particularly important in the photovoltaic (PV) industry where it is used to estimate the energy generation and performance of PV installations. Reliable solar irradiance data is a prerequisite for accurate evaluation of PV projects, as inaccuracy in irradiance estimates can be propagated to, and in some cases exaggerated in, the energy and economic evaluation of a potential project [23]. With the declining price of PV installations, deployment rates have accelerated even in markets such as Norway where the solar insolation is relatively modest [16,29]. It is expected that PV will be a significant energy source in Norway by 2030 [6]. The high expansion rate means that there is an increasing need for high-quality irradiance data. The most reliable and accurate solar irradiance data is generated through local measurements. Such measurements are, however, not always available, for instance for smaller PV installations and during planning of future projects. For such

applications, the solar irradiance must be estimated from other sources.

The extraterrestrial radiation received at the top of the Earth's atmosphere is relatively constant around 1361 W/m² [11]. However, the irradiance reaching the Earth's surface is highly variable. This is due to the diurnal and annual variation of the solar zenith, attenuation of the radiation by clouds, aerosols, and water vapor as well as enhancement of the radiation by ground reflection and cloud lensing. Even in the absence of clouds, the attenuation can be significant. Although the attenuation of radiation from clouds is variable and challenging to predict, the attenuation from aerosols and water vapor is more stable and possible to predict through so-called clear sky models [17,26,22]. Nevertheless, the influence of both these attenuation mechanisms on the irradiance is commonly derived through application of Numerical Weather Prediction (NWP) models or from analyzing satellite imagery.

Historical meteorological parameters such as temperature, wind speed, wind direction, and surface irradiance can be estimated through so-called *reanalysis* in which observational data of the past are combined with NWP models. The methodology allows for the generation of long time series of consistent, gridded global data. The model gridded

* Corresponding author.

E-mail address: Heine.riise@ife.no (H. Nygard Riise).

Abbreviations

BSRN	Baseline Surface Radiation Network
CAMS	Copernicus Atmosphere Monitoring Service
CAMS-Rad	Copernicus Atmosphere Monitoring Service Radiation Service
ECMWF	European Centre for Medium-Range Weather Forecasts
ERA5	European Centre for Medium-Range Weather Forecasts Reanalysis version 5
GHI	Global Horizontal Irradiance
IQR	Interquartile Range
JMA	Japanese Meteorological Agency
JRA55	Japanese 55-year Reanalysis
LMT	Norwegian Agriculture Meteorological Service

masl	meters above sea level
MERRA-2	The Modern-Era Retrospective Analysis for Research and Applications version 2
MET	Norwegian Meteorological Institute (MET)
NASA	National Aeronautics and Space Administration
NWP	Numerical Weather Prediction
POWER	Prediction of Worldwide Energy Resources
PV	Photovoltaic
PVGIS	Photovoltaic Geographical Information System
QC	Quality Control
rMAE	relative Mean Absolute Error
rMBE	relative Mean Bias Error
SARAH-2	Surface Radiation Data Set – Heliosat – Edition 2
TOA	Top Of Atmosphere

reanalysis divides the atmosphere into 3-D grid cells from the surface to the top of the atmosphere. The present most comprehensive global reanalysis is the ERA5 data set with a horizontal resolution of ca. 30 km and 137 levels in the vertical [13]. Other global atmospheric reanalysis datasets include NASA's MERRA-2[8], and JMA's JRA-55[12,21]. The surface irradiance is derived by combining clear sky models with calculations of the cloud cover and short-wave absorption and scattering processes inside a column, i.e., all grid cells above a surface point from the surface to the top of the atmosphere. The presence of clouds is the most significant factor of attenuation of the extraterrestrial radiation. In an NWP model, however, the grid cell volume can be larger than a cloud. Thus, cloud formation and evolvement need to be estimated through parametrization, i.e., by relating the small-scale processes to parameters that can be resolved in the NWP model. This parametrization as well as misrepresentation of the cloud optical thickness introduce uncertainty in the estimation of surface irradiance [18].

A separate approach to estimating solar irradiance is by using remote sensing of the Earth's surface by satellites. By analyzing satellite images, cloud cover, surface albedo and other relevant parameters, the surface irradiance can be extracted. In contrast to reanalysis data where cloud cover is a derived parameter, satellite images can directly sense the cloud cover in an area. The direct sensing is arguably more accurate than reanalysis calculations[35], but satellite generated irradiance estimates also have disadvantages, especially at high latitudes. Most commonly, the surface irradiance is extracted from images generated by geostationary satellites. In Europe, irradiance estimates derived from the Meteosat series, such as CAMS [28,29]and SARAH-2 [27], are commonly used. Geostationary satellites are useful for generating regular and consistent images where the frequency of acquisition is constant, and the viewing angle for a time series of images is the same. This means, however, that the viewing angle gets very high at latitudes above 60°N, complicating the accurate detection of clouds [2,20]. Moreover, the presence of snow on the ground complicates the analysis of satellite images as snow cover can be mistaken for clouds [15]. Thus, solar irradiance estimates from satellite images at high latitude locations are associated with higher inaccuracy than for locations closer to the equator.

Many studies have been carried out to benchmark estimated solar irradiance data products, showing typically that satellite-derived irradiance products outperform reanalysis irradiance products [35,25,34,30,3]. A significant proportion of these studies utilize ground measured irradiance data from well-maintained and top-standard stations from the Baseline Surface Radiation Network (BSRN), ensuring that the ground measured data is of high quality. The distribution of the BSRN stations, however, precludes wide-spread validation north of 60°N, and hence, benchmarking studies of estimated solar irradiance at such latitudes are sparse. The ones that have been conducted have highlighted that the accuracy of the irradiance products depends on the

latitude and the cloudiness of the ground site [31,2,4,20].

The following study compares six different sources of estimated solar irradiance towards measurements conducted at 34 ground stations scattered across Norway. The ground stations are located at latitudes ranging between 58°N and 76°N. The solar irradiance sources considered are based on both reanalysis and satellite images. The ground stations are equipped with class A pyranometers that are rigorously quality controlled.

2. Methods

2.1. Ground data description

The benchmark is performed by comparing six sources of estimated irradiance to global horizontal irradiance (GHI) measured by class A pyranometers at 34 ground stations scattered across Norway. The pyranometers have an uncertainty of +/- 2 % [33]. Fig. 1 shows the location of all the stations together with the mean annual irradiation in the period 2016 – 2020, while Table 1 lists the location, altitude, mean annual irradiation, number of months with median snow depth above 0 cm, Köppen–Geiger climate zone, and median clearness index over the whole analysis period, i.e., the measured GHI divided by the extraterrestrial radiation. The validation period is from January 1st, 2016, to December 31st, 2020. The analysis period was chosen since a number of ground stations came online in 2015, while some of the data products do not provide data after 2020. All stations have a data coverage where more than 96 % of the possible, hourly data points are in the data set, while every month in the validation period also contains more than 84 % of its possible, hourly data points. As can be seen from Fig. 1, the highest annual irradiation is found in South-East Norway, which is also where the density of stations is highest. Most of the stations are operated by the Norwegian Agriculture Meteorological Service (LMT). The stations at Jan Mayen and Hopen are operated by the Norwegian Meteorological Institute (MET). The stations undergo at least biennial maintenance and regular cleaning. The GHI is recorded by the pyranometer once a minute, but in the present work the data is aggregated to hourly mean values.

2.2. Quality control

The GHI data has been thoroughly quality checked, both by automated filters and manual inspection. The automated methods include eight tests listed in Table 2. The tests ensure that all GHI values are physical by not significantly exceeding the theoretical maximum (tests "TOA" and "Clear sky"), or that they have.

unphysically low values during nighttime or daytime (tests "Offset," "Low," and "Negative"). Additionally, there are tests to ensure that the variation and distribution of the data is as expected ("Difference,"

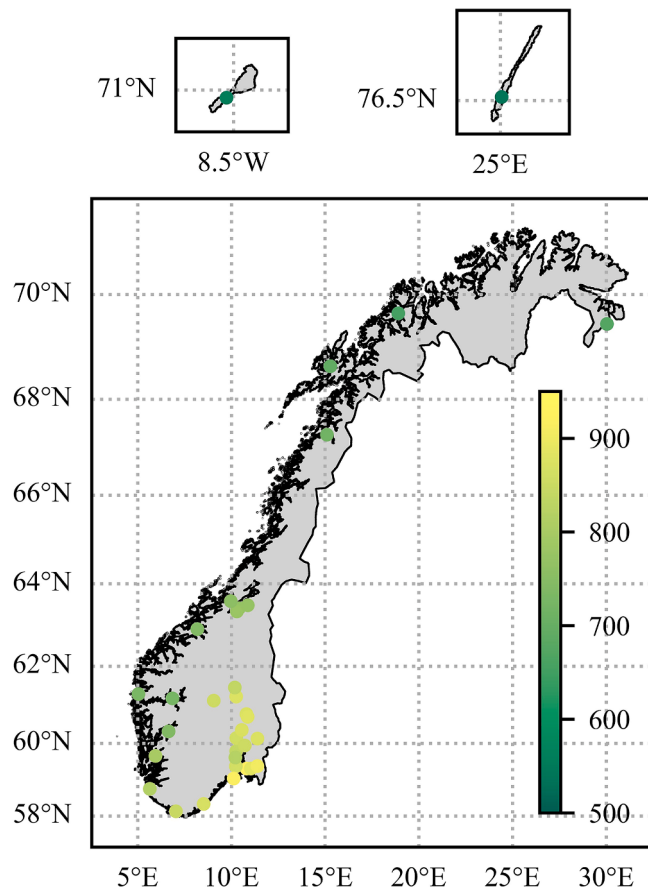


Fig. 1. Position and mean annual irradiation of the ground stations of this study. The circle color indicates the mean annual irradiation in the period 2016–2020.

“Consistency”). The tests are based on previous work [10,19] for low elevated stations around the Oslofjord but have been refined in this work to cover the whole of Norway. The refinement from previous work most importantly results in an adjustment of the upper limit function in the clear sky test, fitting it to the varying conditions of around 100 different stations throughout Norway. The refinement work led to a clear sky filter which treats low and high clear sky irradiances differently (cf. Fig. 2). For the quality control (QC) and filtering procedure, the clear sky irradiance is estimated by the CAMS McClear clear sky Radiation service [5], [22]. Basing the QC on observations of turbidity through McClear instead of table lookups arguably improves the accuracy of the clear sky radiation and the QC procedures. Any data point that is captured by the tests is discarded from the validation. Filtering removes between 6 % and 23 % of the daytime values, depending on the station.

The tests in Table 2 flag nonphysical and inconsistent values in the data (Figure A1 in the appendix). In addition, it is necessary to catch other types of problems with the sensors, e.g., drift, shading, and bad calibration. To detect these types of issues, the following comprehensive visual inspection methods were applied pointing out issues that may need further investigation [7]:

- 1) Time-series of measured GHI (Figure A1 in the appendix). Such figures enable detection of issues like negative trends or implausible differences between nearby stations.
- 2) Diurnal and annual cycle of measured and clear sky GHI displayed as heat-maps (Figure A2 in the appendix). Such figures can aid in the detection of shading which is visible as sharp horizontal gradients. Moreover, small positive or negative values during night can point to calibration issues. For the stations shown in Figure A2 in the

appendix, issues with missing data and nighttime offsets can be seen as white and grey sections.

- 3) Measured/clear sky radiation ratio presented as scatter plots (Fig. 2). These figures can reveal unreasonably high values in the measurements. Note that the observed values are generally lower than the clear sky values due to clouds reducing the radiation received at the surface. Many measurements exceeding the clear sky values with a factor of 1.3 indicates doubtful data. As seen in Fig. 2, the data from Østre Toten – Apelsvoll mostly is below the limits, while the Skjetlein data has a large number of points outside the clear sky filter, indicating more issues with the Skjetlein station compared to the Østre Toten – Apelsvoll station.
- 4) Frequencies of measured/clear sky GHI ratios shown as histograms give a summary of the ratio between measured and clear sky GHI (Fig. 3). Ideally, the frequencies should show a clear peak around 1 for years with sufficient hours of fair weather and a steep drop above 1. If the peak is too weak or have many values above 1, this is an indication of issues with the data. Like in Fig. 2, the data in Fig. 3 indicates that the Skjetlein station has more problems than the Østre Toten – Apelsvoll station, as the peak around 1 is less sharp.

2.3. Estimated data description

Six different estimated solar irradiance data products are compared in this study. The data products are summarized in Table 3 where their differences in methodology and source of radiation information is highlighted.

As seen in Table 3, three of the products (CAMS radiation, PVGIS SARAH-2 and Solargis) do not offer radiation estimates above 65°N/66°N. This is because these data products are mainly based on geostationary satellite imagery, and at high latitudes the viewing angle of the satellite is too large to achieve reliable irradiance estimates. The three products are in the following referred to as the geostationary satellite products. The other three data products have a larger coverage, either because they do not rely on satellite imagery (PVGIS ERA5), or they utilize other sources of data at high latitudes. For instance, Meteonorm interpolates between ground stations using ERA5-data above 62°N, while NASA POWER relies on both polar-orbiting satellites and reanalysis datasets. There is also a difference between the spatial resolution that is offered. PVGIS ERA5 and NASA POWER have a coarse spatial resolution of 0.25°x0.25° and 1°x1°, respectively, while PVGIS SARAH-2 offer a finer resolution of 0.05°x0.05°. The other data products can offer interpolation to the point in question, but the input data to the models have varying spatial resolution. For instance, input of aerosol properties to CAMS has a spatial resolution of 0.4°x0.4° (approximately equal to 22 × 44 km² at 60°N), while input of cloud properties has a spatial resolution of 3 × 3 to 10 × 10 km². Although the data products can offer horizon correction through different surface models, that is not utilized in the following analysis.

2.4. Metrics

Performance is characterized through the mean absolute error (*MAE*) and mean bias error (*MBE*). *MAE* and *MBE* are normalized to the mean GHI value at each individual station and denoted *rMAE* and *rMBE* to indicate they are relative values [14]:

$$rMAE = \frac{\sum_{i=1}^n |y_{p,i} - y_i|}{n} / \frac{\sum_{i=1}^n y_i}{n} \quad (1)$$

$$rMBE = \frac{\sum_{i=1}^n y_{p,i} - y_i}{n} / \frac{\sum_{i=1}^n y_i}{n} \quad (2)$$

where y_i is the observation at time i , $y_{p,i}$ is the estimated irradiance at time i , and n is the number of observations. All observations fulfill the criteria described in Table 2, and are thus daytime values.

Table 1

Description of stations that are part of the present work.

Station Name	Latitude (°N), Longitude (°E)	Altitude (MASL)	Mean Annual Irradiation (kWh/m ² /yr)	Months per year with median snow depth > 0 cm	Köppen –Geiger Climate Zone	Median clearness index
Lyngdal	58.14, 7.05	6	847	0	Cfb	0.30
Landvik	58.34, 8.52	6	867	1	Cfb	0.31
Særehem	58.76, 5.65	87	815	0	Cfb	0.29
Tjølling	59.05, 10.13	19	917	0	Cfb	0.36
Råde – Tomb	59.32, 10.81	12	921	0	Cfb	0.36
Øsaker	59.32, 11.04	45	888	0	Cfb	0.35
Ramnes – Kile Vestre	59.38, 10.24	39	865	3	Cfb	0.33
Rakkestad	59.39, 11.39	100	907	2	Cfb	0.33
Sande – Galleberg	59.62, 10.22	60	822	4	Cfb	0.29
Etne II	59.66, 5.95	8	799	0	Cfb	0.30
Lier	59.79, 10.26	39	840	3	Dfb	0.31
Oslo – Blindern	59.94, 10.72	94	853	2	Dfb	0.33
Årnes	60.13, 11.39	160	874	4	Dfb	0.33
Hønefoss – Hverven	60.14, 10.27	126	859	4	Dfb	0.34
Ullensvang	60.32, 6.65	12	741	0	Cfb	0.24
Forsøksgard						
Gran	60.36, 10.56	245	872	4	Dfb	0.35
Østre Toten – Apelsvoll	60.70, 10.87	264	881	4	Dfc	0.33
Kise på Hedmark	60.77, 10.81	128	874	4	Dfb	0.32
Løken i Volbu	61.12, 9.06	521	853	6	Dfb	0.32
Njøs	61.18, 6.86	45	724	0	Cfb	0.24
Gausdal – Follebu	61.22, 10.26	375	875	5	Dfc	0.34
Fureneset	61.29, 5.04	7	729	0	Cfb	0.24
Fåväng	61.46, 10.18	200	836	5	Dfc	0.31
Tingvoll	62.91, 8.19	23	742	0	Dfc	0.28
Skjetlein	63.34, 10.30	48	779	3	Cfc	0.33
Trondheim – Gløshaugen	63.42, 10.41	60	773	3	Cfb	0.33
Kvitthamar	63.49, 10.88	27	771	3	Cfb	0.29
Rissa III	63.59, 9.97	23	757	0	Cfc	0.30
Valnesfjord	67.28, 15.10	20	717	4	Dfc	0.30
Sortland – Kleiva	68.65, 15.28	14	691	5	Dfc	0.28
Pasvik – Svanvik	69.46, 30.04	27	671	6	Dfc	0.28
Tromsø – Holt	69.65, 18.91	20	654	7	Dfc	0.26
Jan Mayen	70.94, -8.67	10	556	No data	ET	0.23
Hopen	76.51, 25.01	6	541	No data	ET	0.26

Table 2Automatic filters implemented in the quality control of the ground measured data. Θ = Solar zenith angle, I_E = Extraterrestrial solar irradiance, I_{CS} = clear sky irradiance, σ = variance, μ = mean.

Test	Criteria
Offset	$GHI > 6 \text{ W/m}^2$ if $\theta > 93^\circ$
TOA	$GHI > I_E$
Clear sky	$GHI > f \times I_{CS} + a$, where $f = 2$, $a = 0$ if $I_{CS} \leq 100 \text{ W/m}^2$; or $f = 1.05$, $a = 95$ if $I_{CS} \geq 100 \text{ W/m}^2$
Low	$GHI < 10^{-4} \times (80 - \theta) \times I_E$ if $\theta \leq 80^\circ$
Difference	$\frac{d(GHI/I_E)}{dt} \geq 0.75$ if $\theta < 80^\circ$
Consistency	$\sigma(GHI/I_E) < 1/16 \times \mu(GHI/I_E)$; or $\sigma(GHI/I_E) > 80$
Missing	$GHI = \text{N/A}$
Negative	$GHI <= 0$

3. Results

3.1. Overall

Fig. 4 presents the $rMBE$ and $rMAE$ comparing the hourly measured irradiance from the 34 ground stations to corresponding estimated values provided by the six different solar irradiance data products.

The horizontal line inside the boxes highlights the median (Q_2) of the distribution, the box edges show the first (Q_1) and third (Q_3) quartiles, the lower whisker indicates $Q_1 - 1.5 \times IQR$, while the upper length indicates $Q_3 + 1.5 \times IQR$ where $IQR = Q_3 - Q_1$ is the interquartile range. The median $rMAE$ ranges between 18.6 and 27.1 % for the different data

products. The median $rMBE$ is in the range -0.2–6.0 %. The $rMBE$ values are comparable to benchmarks carried out at lower latitudes but the $rMAE$ values reported here are higher than what is reported at lower latitudes [35,31], highlighting the challenges of high latitude irradiance estimation. Similar conclusions can be drawn from previous benchmarks at high latitudes [2,4,20]. However, the distributions show that there is large variation in performance, both in terms of $rMAE$ and $rMBE$, between the different stations. Fig. 4 shows that the estimated irradiance from Meteonorm, PVGIS ERA5, and NASA POWER in general tends to overestimate the irradiance, i.e., there is a positive bias in the median of the distribution of $rMBE$. For CAMS, PVGIS SARAH-2 and Solargis the bias is typically smaller, with the median of the $rMBE$ -distribution close to 0. By considering the whisker extent of the figure, however, it can be seen that these products can reach $rMBE$ up to +/- 10 % for individual locations. The relative performance of CAMS, PVGIS SARAH-2 and Solargis is similar as in a comparable study from the United Kingdom, albeit with a previous version of SARAH [25]. The study, however, displays a significantly lower accuracy for CAMS and SARAH than what is found in the present work. CAMS, PVGIS SARAH-2 and Solargis all have in common that they are mainly based on remote sensing from high-resolution, geostationary satellites, which previously has been shown to provide the most accurate irradiance estimates in lower latitudes [35]. The overestimation of irradiance by PVGIS ERA5 has been reported previously and could stem from failures related to clouds and their composition [32]. The higher accuracy of the geostationary satellite products is also reflected in 3–9 %_{abs} lower $rMAE$ than the other products, i.e., a median of 18.6–20.3 % compared to 22.4–27.1 %.

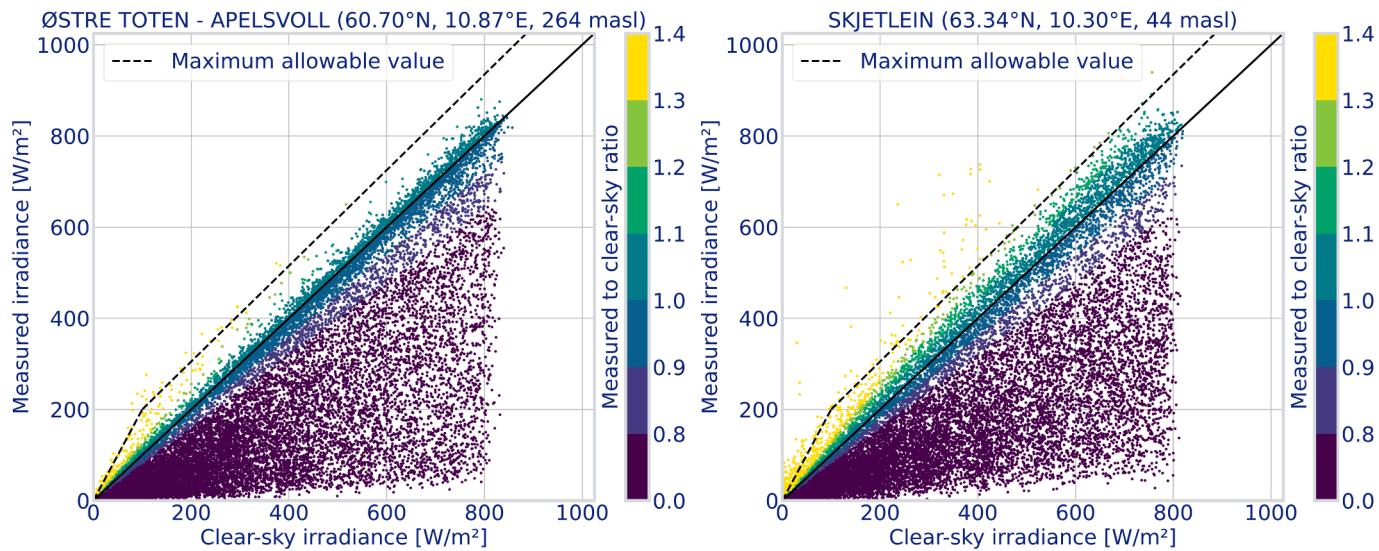


Fig. 2. Scatterplots of measured (y-axis) and estimated clear sky irradiance (x-axis) for the Østre Toten – Apelsvoll (left) and Skjælein (right) station. Colors indicate the ratio of measured to clear sky irradiance. The black solid line is a guide to the eye where GHI/ICS = 1.

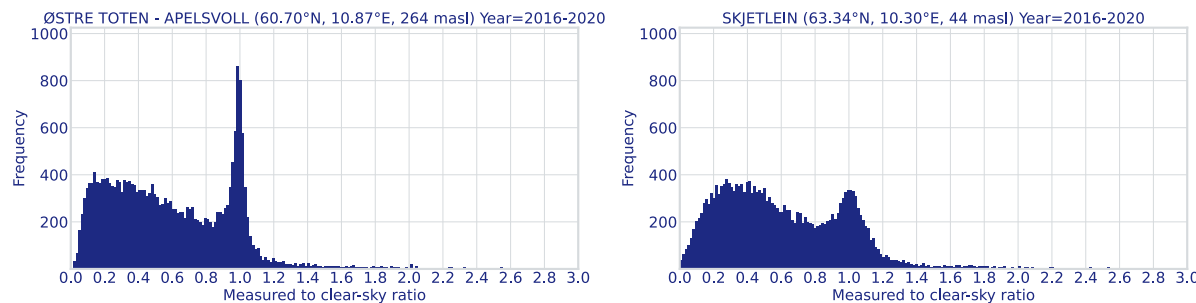


Fig. 3. Histograms of measured to clear sky irradiance ratios for the Østre Toten – Apelsvoll (left) and Skjælein (right) station.

Table 3

Overview and characteristics of the modelled estimated solar irradiance data products that are benchmarked in this study.

Estimated solar irradiance product	Source	Spatial availability (°N, °E, °S, °W)	Spatial resolution	Temporal resolution	Temporal availability	Relevant resources
CAMS radiation	High-resolution geostationary satellite imagery	66, 66, -66, -66	Interpolated to point of interest	15 min	2004–2 days ago	[28,22], https://atmosphere.copernicus.eu/solar-radiation-supplementary-products
PVGIS SARAH-2	High-resolution geostationary satellite imagery	65, 65, -65, -65	0.05°x0.05°	30 min	2005–2020	[9] https://re.jrc.ec.europa.eu/pvg_tools/en/
Solargis	High-resolution, geostationary satellite imagery	Global up to 65°N/S	Interpolated to point of interest	15 min	1994–now	https://solargis.com/products/evaluate
Meteonorm	Ground stations, interpolation between stations (satellite < 62°N atmospheric reanalysis > 62°N)	Global	Interpolated to point of interest	60 min	2008–1 month ago	https://meteonorm.com/en/meteonorm-documents
PVGIS ERA5	Atmospheric reanalysis	Global	0.25°x0.25°	60 min	2005–2020	[13], https://re.jrc.ec.europa.eu/pvg_tools/en/
NASA POWER	Satellite imagery, atmospheric reanalysis	Global	1°x1°	60 min	1984–7 days ago	https://power.larc.nasa.gov/

3.2. Impact of latitude and cloudiness

The high-resolution, geostationary satellite irradiance products do not provide irradiance estimates above 65°N due to the high viewing angles. This generates a bias in the overall results as Meteonorm, PVGIS ERA5, and NASA POWER in general perform worse at high latitudes. This is seen in Fig. 5 where the *rMAE* is higher north of 65°N for all three NWP products compared to below 65°N.

For Meteonorm and NASA POWER, *rMBE* is also generally higher.

Especially Meteonorm has a lower accuracy at higher latitudes, with 9.4 percentage points higher median *rMAE* and 5.6 percentage points higher median *rMBE*. The lower accuracy at high latitudes could come from a poor estimation of the radiation reflection from snow, as the high latitude stations have a higher prevalence of snow on the ground (see Table 1). The stations at latitudes above 65°N also experience a median clearness index over the whole 5-year period of 0.27 with a range of 0.23 – 0.30. That is significantly lower than the low latitudes stations that have a median clearness index of 0.32 and *IQR* in the range 0.29 – 0.33.

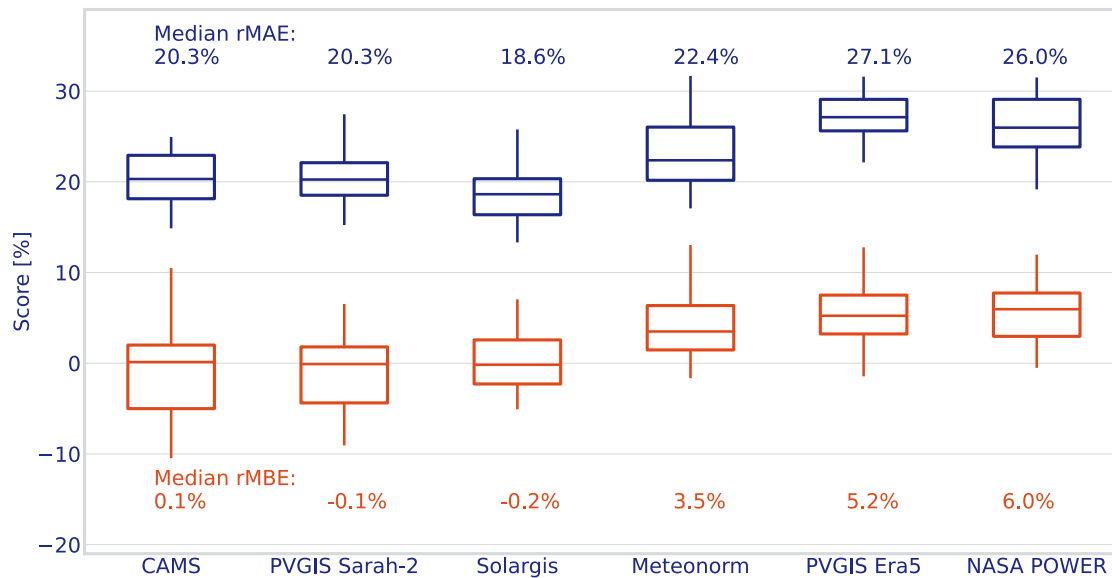


Fig. 4. rMAE (blue, upper boxes) and rmbe (orange, lower boxes) of all the stations in the study. The median rMAE and rmbe for each data product is displayed in the top and bottom of the figure, respectively. (For interpretation of the references to color in this figure legend, the reader is referred to the web version of this article.)

A lower clearness index indicates more cloudy weather, which is known to reduce the accuracy of estimated irradiance [32,25]. The effect is also seen in the left-hand panel of Fig. 6 where the rMAE of the different irradiance products are shown as a function of the median clearness index.

In Fig. 6, the rMAE reduces with higher median clearness index demonstrating that the accuracy of the estimated irradiance is dependent on the cloudiness. In the right-hand panel of Fig. 6, a clear dependency of rMAE on latitude can be seen, in line with observations from previous benchmarks [31,25,2]. The dependency is strong also for latitudes below 65°N. This is also the case for PVGIS ERA5 that is derived from reanalysis and should, in principle, not be affected by the viewing angle of geostationary satellites.

By excluding the stations above 65°N, the performance relative to including all stations of Meteonorm and PVGIS ERA5 stay similar, the change in median rMAE and rmbe is in the range 0.0 – 0.5 percentage points, cf. the values south of 65°N that are printed in Fig. 4 and Fig. 5. For Meteonorm, this might be counterintuitive as the performance at higher latitudes is significantly weaker than at lower latitudes. It should be stressed, however, that the discussion here revolves around the median of the distribution which is robust against outliers such as the stations above 65°N. The NASA POWER performance improves with 2.3 percentage points reduction in rmbe and 0.8 percentage points reduction in rMAE, cf. the values south of 65°N in Fig. 4 and Fig. 5. Nonetheless, the rmbe of all three models are still positive south of 65°N indicating that they on average overestimate the irradiance that a station receives. Note that the geostationary satellite products are not shown in Fig. 5 since they do not provide data above 66°N.

3.3. Impact of horizon shading and snow

As discussed in the previous paragraphs, snow can have an impact on the accuracy of the estimated irradiance. To further illustrate this point, Fig. 7 compares the rMAE and rmbe between snowy and non-snowy stations.

For the classification, a snowy station is assumed to be at a location where the median monthly snow depth on the ground is higher than 0 cm for at least five months of the year. Data about snow depth is based on interpolated observational data is collected from seNorge.no [24]. CAMS, PVGIS ERA5, PVGIS SARAH-2, and Solargis all display a lower

median bias at the snowy stations as compared to the non-snowy stations. This indicates that the products estimate lower irradiance at snowy stations than at non-snowy stations. Note that the products have a median bias close to 0 for the non-snowy station. Although NASA POWER and Meteonorm do not have a lower median bias at snowy stations, all the irradiance products have lower precision in snowy conditions. This is reflected by the higher rMAE for the snowy stations compared to the non-snowy stations.

The cause of the poor estimation of irradiance at snowy locations is at least two-fold. In addition to poor estimation of the radiation reflection from the snow mentioned above, the satellite-based products is also known to struggle with distinguishing snow on the ground from cloud cover [15,1,31]. This will especially affect CAMS, PVGIS SARAH-2 and Solargis since they depend on geostationary satellite data. In principle it should also affect NASA POWER, but it appears that the coarse resolution of NASA POWER masks the problem. The misidentification of snow cover as clouds is illustrated in Fig. 8 where three clear sky days in April 2019 are displayed for a station located in a mountain area in southern Norway.

The ground is covered in snow, as confirmed by senorge.no. On April 10th and April 11th, 2019, CAMS estimates significantly lower irradiance than what is measured indicating that the snow cover is misinterpreted as cloud cover. On the afternoon of April 10th, there is broken cloud conditions, leading to a significant drop in the estimated irradiance of CAMS. On April 12th, PVGIS SARAH-2 and Solargis underestimate the irradiance, and especially PVGIS SARAH-2 interpret the snow cover as a thick cloud at 13:00. These three days demonstrate how prone satellite-based irradiance products are to misinterpreting snow as clouds, and how sensitive their methods are to small changes in the imagery.

In addition to snow and high satellite viewing angle, the rugged topography of Norway is a complicating factor for correctly estimating the irradiance [1]. Especially the fjord regions in western Norway have terrain where the sun can be shaded by the horizon for extended times of the day throughout the whole year. An example is shown in Fig. 9 where the pyranometer at the station Njøs in Sognefjorden is shaded for four hours in the morning.

Note that the date is July 4th, 2018, which is close to the summer solstice. This can be corrected by adding a horizon mask, but to leave the results as unaffected by analyst choices as possible this is not done here.

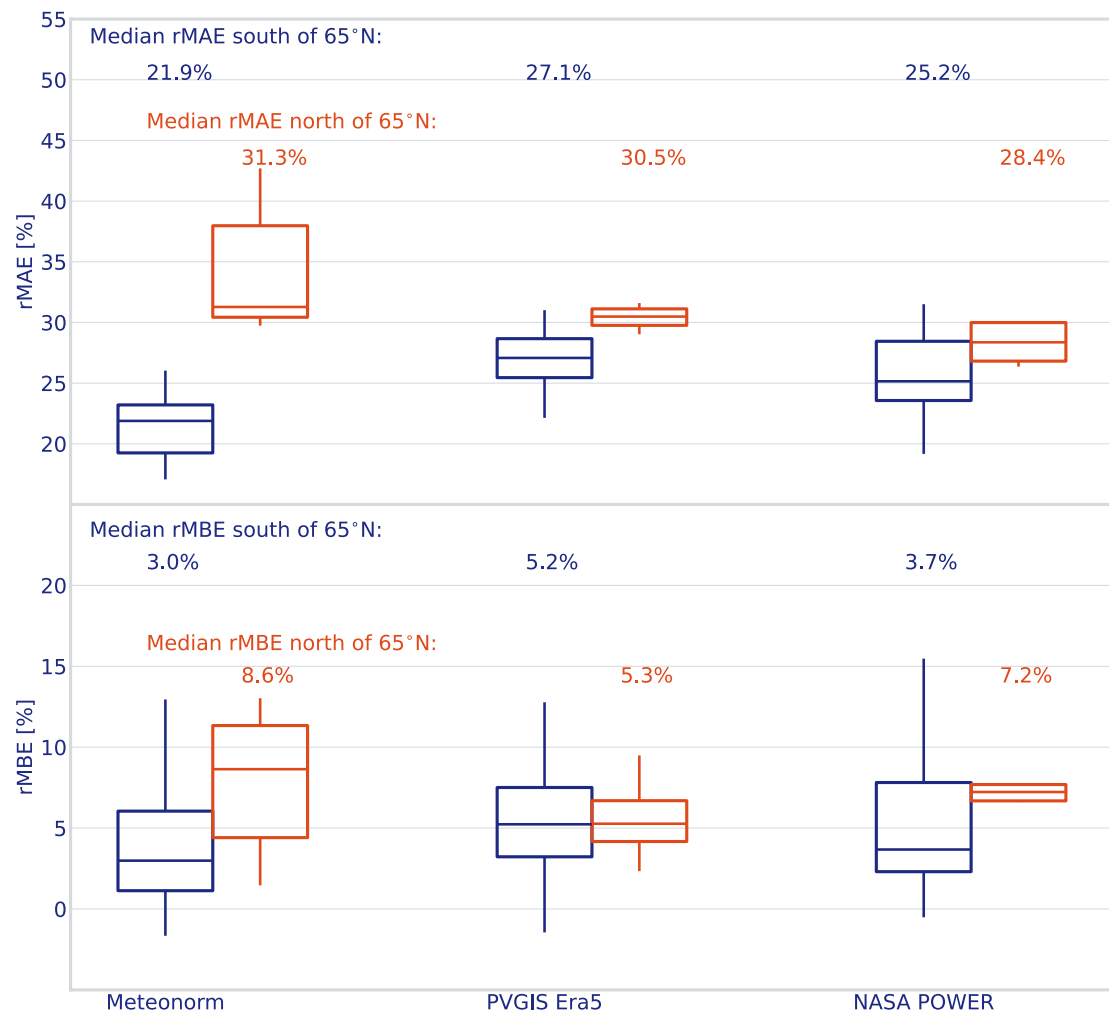


Fig. 5. rMAE and rMBE south (blue boxes) and north (orange boxes) of 65°N. The figure only includes PVGIS ERA5, Meteonorm and NASA POWER since the geostationary satellite products do not provide data above 65°N. The median accuracy and precision of the data products are significantly higher in lower latitudes. The exception is PVGIS ERA5, where the median rMBE is approximately the same between low and high latitudes. (For interpretation of the references to color in this figure legend, the reader is referred to the web version of this article.)

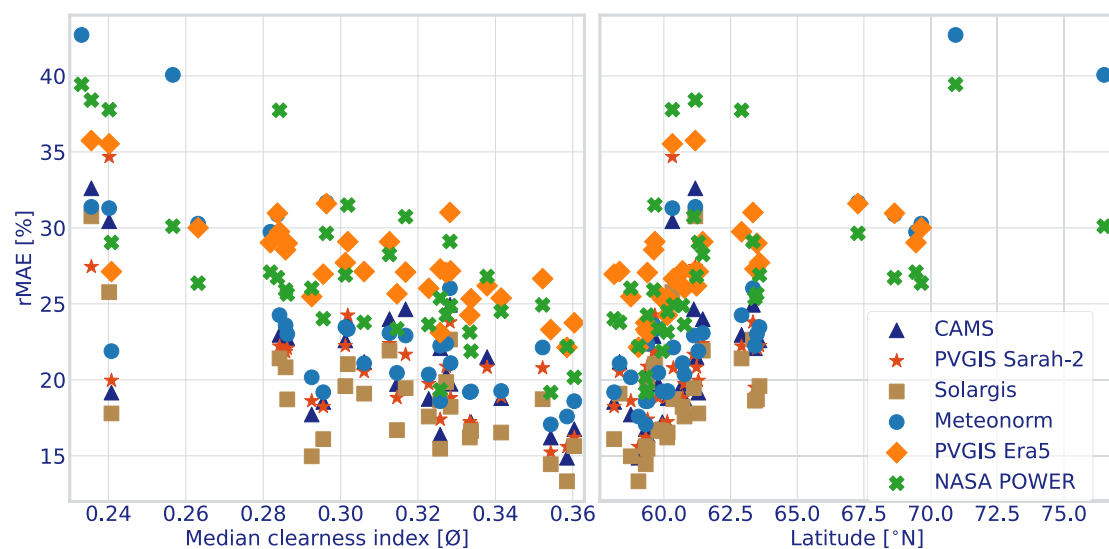


Fig. 6. rMAE dependency on clearness and latitude. The trends in the figures illustrate the challenges of estimating irradiance at high latitude and in cloudy conditions as the accuracy degrades with higher latitudes and lower clearness index.

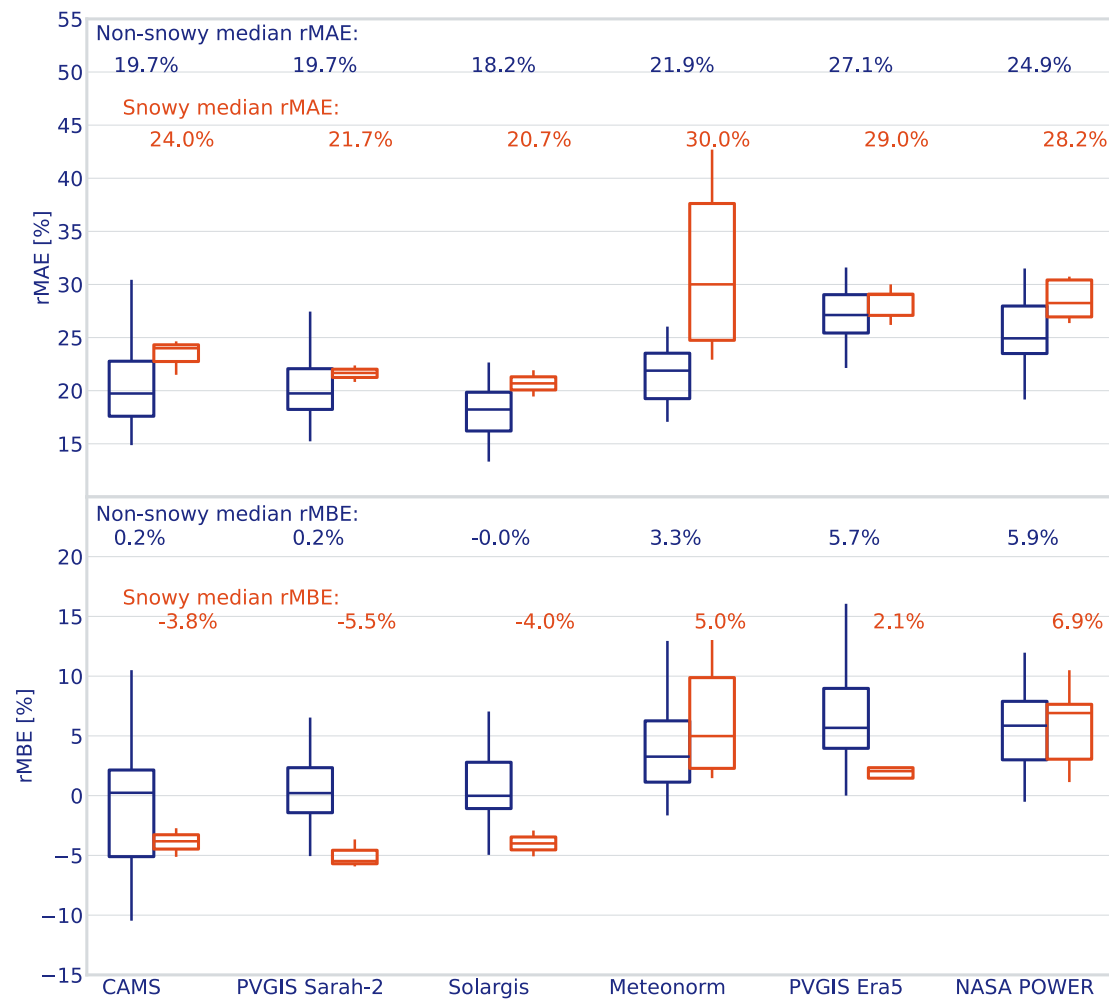
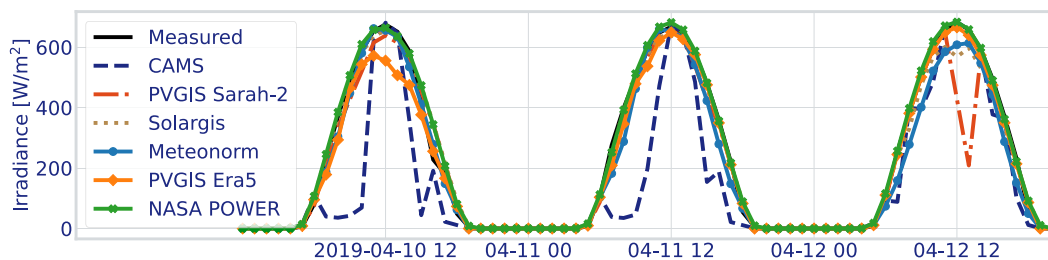


Fig. 7. rMAE and rMBE for non-snowy (blue boxes) and snowy (orange boxes) sites. The rMAE is higher for the snowy sites as compared to the non-snowy sites. Moreover, most of the data products display a lower bias at the snowy sites compared to the non-snowy sites. The exception is Meteonorm and NASA POWER where the median rMBE is higher for the snowy sites. (For interpretation of the references to color in this figure legend, the reader is referred to the web version of this article.)



To get an impression of the irradiance estimates without significant impact related to snow, horizon shading and high latitudes, Fig. 10 shows the *rMAE* and *rMBE* where all the snowy, horizon shaded, and high latitude sites are filtered out. This leaves a total of 23 measurement stations with latitudes ranging between 58°N and 63°N. Fig. 10 demonstrates that the median *rMBE* of PVGIS SARAH-2 and Solargis is close to zero, while CAMS, Meteonorm, PVGIS ERA5, and NASA POWER in general exhibit positive bias. Furthermore, with a median *rMAE* below 18 %, Solargis are seen to have the highest average accuracy in estimating the irradiance at the 23 stations.

4. Conclusions

This study has benchmarked six different irradiance data products, CAMS, PVGIS SARAH-2, Solargis, Meteonorm, PVGIS ERA5, and NASA POWER, to hourly, ground measured data from 34 stations in Norway. A rigorous quality control is applied to the ground measured data, including a requirement of measurements from class A pyranometers.

Overall, the data products that are based on high-resolution, geostationary satellites (CAMS, PVGIS SARAH-2, and Solargis) follow the ground measurements most closely with median *rMAE* around 20 % and

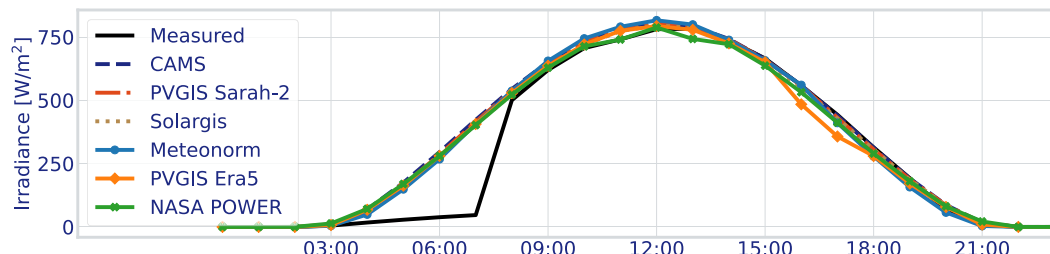


Fig. 9. Irradiance time series from the station Njøs in Sognefjorden from July 4th, 2018. The station is horizon shaded in the morning, leading to a positive bias for the irradiance data products.

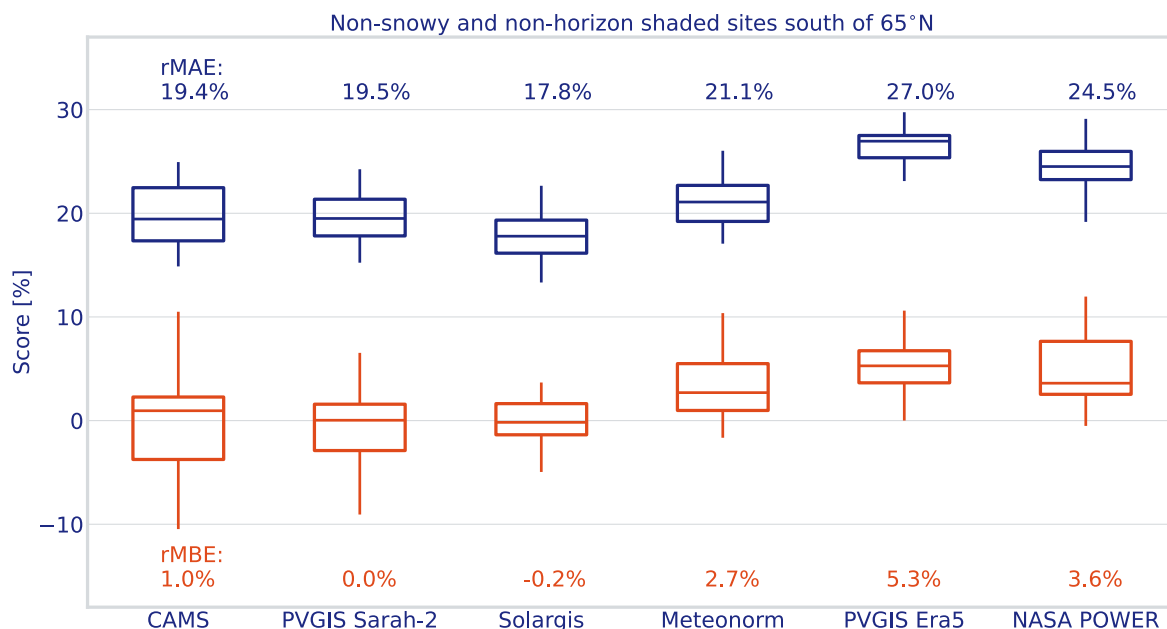


Fig. 10. rMAE (blue, upper boxes) and rMBE (orange, lower boxes) of stations south of 65°N that are not horizon shaded or significantly snow affected. (For interpretation of the references to color in this figure legend, the reader is referred to the web version of this article.)

median *rMBE* around 0 %. Meteonorm, PVGIS Era5 and NASA POWER have a slightly lower performance with median *rMAE* between 22.4 and 27.1 % and median *rMBE* between 3.5 and 6.0 %. The performance of all data products is demonstrated to depend on the latitude and the median clearness index at the different ground station locations. The highest station median clearness index for the whole analysis period is 0.36, indicating quite cloudy conditions for all the stations. As irradiance estimates are more uncertain in cloudy conditions, the low clearness indices and high latitudes illustrates the challenges with estimating irradiance in Norway. Challenges related to snow and horizon shading is also discussed, where the latter is especially pronounced in the rugged fjord terrain of Western Norway. Satellite based irradiance estimation can have issues with misinterpreting snow as cloud cover, and this is indeed demonstrated for CAMS and PVGIS SARAH-2.

Excluding stations that are significantly horizon shaded, have snow on the ground for extended periods of the year, or are located above 65°N , the trends from including all stations are still valid: CAMS, PVGIS SARAH-2 and Solargis have the highest accuracy with median *rMAE*

below 20 %, while Meteonorm, PVGIS ERA5, NASA POWER have positive median *rMBE* of more than 2.7 %.

CRediT authorship contribution statement

Heine Nygard Riise: Writing – original draft, Methodology, Investigation, Formal analysis, Data curation, Conceptualization. **Magnus Moe Nygård:** Writing – review & editing, Methodology. **Bjørn Lupton Aarseth:** Writing – review & editing. **Andreas Dobler:** Writing – review & editing, Methodology, Data curation. **Erik Berge:** Writing – review & editing, Methodology, Data curation, Conceptualization.

Acknowledgements

The authors gratefully acknowledge funding from the Research Council of Norway (KPN SUNPOINT, grant. no 320750). A sincere thanks to Dr. Marit Sandsaunet Ulset for valuable revisions and discussions.

Appendix 1

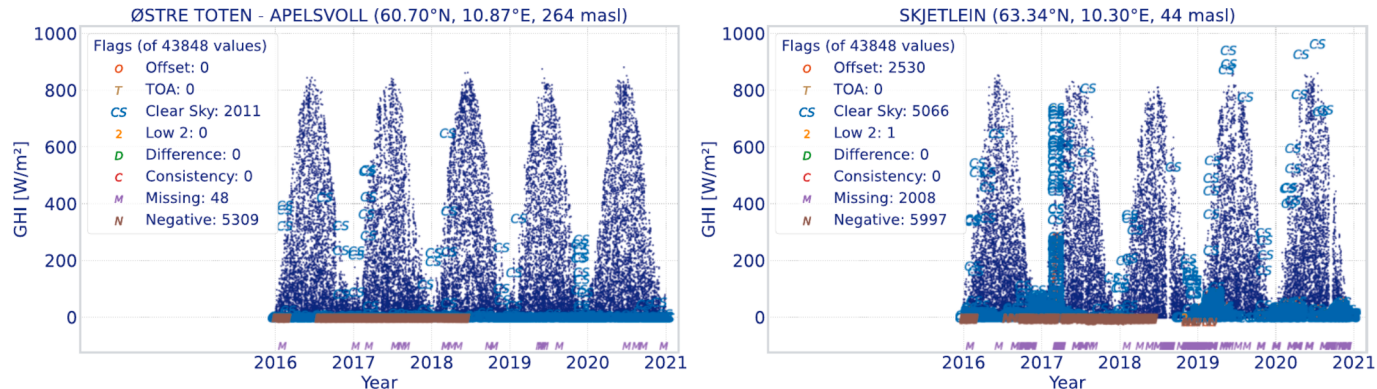


Fig. A1. Time series and flags assigned by the automated tests for the Østre Toten – Apelsvoll (left) and Skjettlein (right) station data.

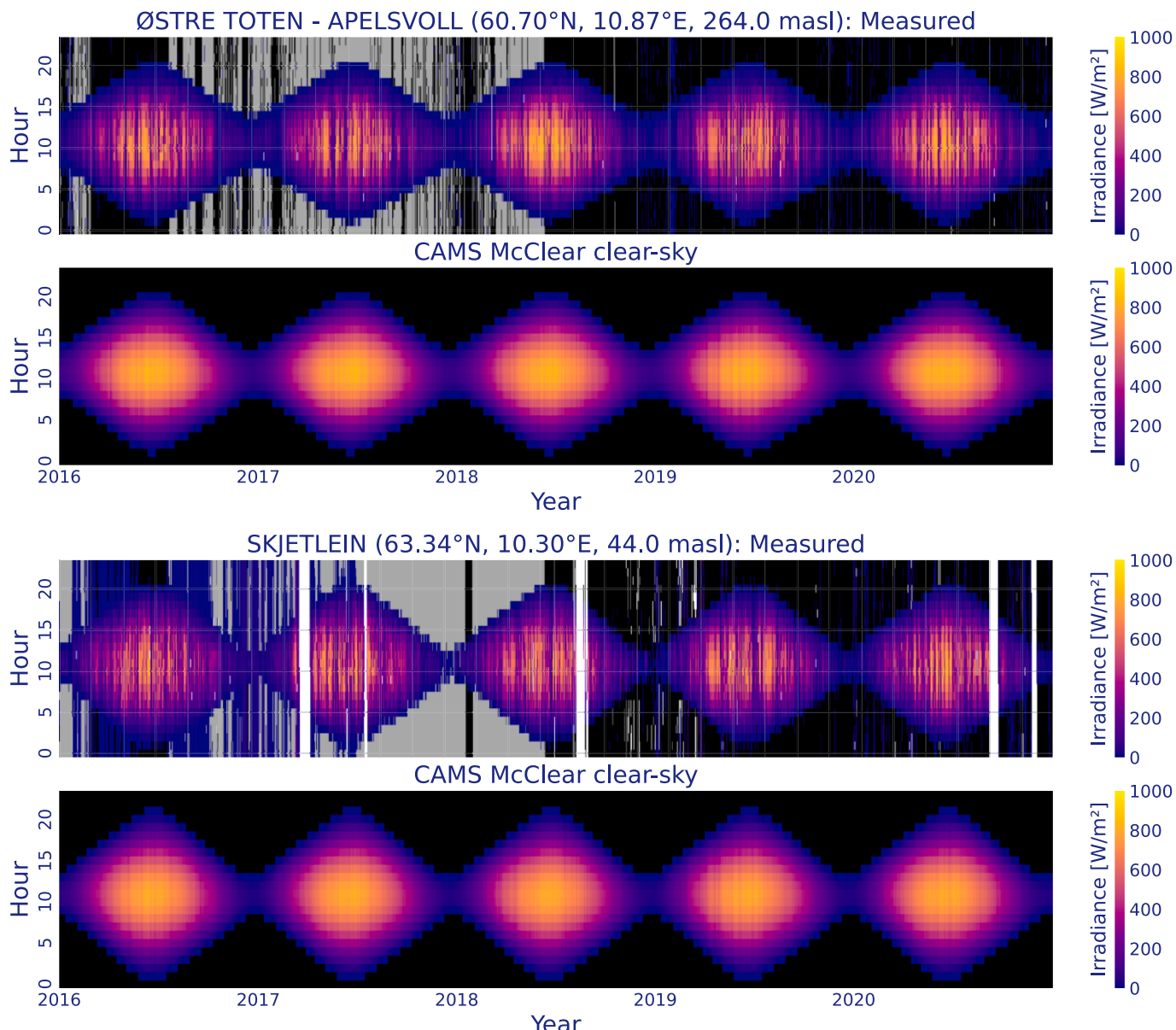


Fig. A2. Heat-map visualization for the Østre Toten – Apelsvoll (top) and Skjettlein (bottom) station. Days are given on the x-axis and hour of the days on the y-axis. The top rows show the measured data while the lower rows show the clear sky estimates at the location. Zero values are shown in

black, negative values in gray and missing values in white.

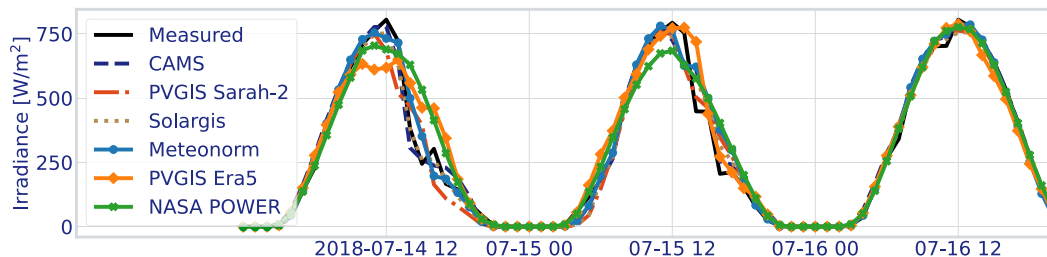


Fig. A3. Irradiance time series from the ground station Løken i Volbu from three clear-sky days in July 2018. Illustration that when the ground is not snow-covered, the geostationary satellite products (PVGIS SARAH-2, CAMS and Solargis) can accurately estimate the irradiance.

References

- [1] B. Babar, R. Graversen, T. Boström, Evaluating CM-SAF solar radiation CLARA-A1 and CLARA-A2 datasets in Scandinavia, *Sol. Energy* 170 (2018) 76–85.
- [2] B. Babar, R. Graversen, T. Boström, Solar radiation estimation at high latitudes: assessment of the CMSAF databases, ASR and ERA5, *Sol. Energy* 182 (2019) 397–411.
- [3] J.M. Bright, Solcast: validation of a satellite-derived solar irradiance dataset, *Sol. Energy* 189 (2019) 435–449.
- [4] P.E. Campana, T. Landelius, S. Andersson, L. Lundström, E. Nordlander, T. He, J. Zhang, B. Stridh, J. Yan, A gridded optimization model for photovoltaic applications, *Sol. Energy* 202 (2020) 465–484.
- [5] “CAMS solar radiation time-series. Copernicus Atmosphere Monitoring Service (CAMS) Atmosphere Data Store (ADS).” (Accessed on 01-02-2023), <https://ads.atmosphere.copernicus.eu/cdsapp#!/dataset/cams-solar-radiation-timeseries?tab=overview>. In.
- [6] Energikommisjonen. 2023. “Mer av alt - raskere.” In.
- [7] Forstinger, Anne, Stefan Wilbert, Adam Jensen, Birk Kraas, Carlos Fernández Peruchena, Chris A. Gueymard, Dario Ronzio, Dazhi Yang, Elena Collino, Jesús Polo Martínez, Jose A. Ruiz-Arias, Natalie Hanrieder, Philippe Blanc, and Yves-Marie Saint-Drenan. 2021. “Expert quality control of solar radiation ground data sets.” In *ISES Solar World Congress*.
- [8] R. Gelaro, W. McCarty, M.J. Suárez, R. Todling, A. Molod, L. Takacs, C.A. Randles, A. Darmenov, M.G. Bosilovich, R. Reichle, K. Wargan, L. Coy, R. Cullather, C. Draper, S. Akella, V. Buchard, A. Conaty, A.M. da Silva, Gu. Wei, G.-K. Kim, R. Koster, R. Lucchesi, D. Merkova, J.E. Nielsen, G. Partyka, S. Pawson, W. Putman, M. Rienercer, S.D. Schubert, M. Sienkiewicz, B. Zhao, The modern-era retrospective analysis for research and applications, version 2 (MERRA-2), *J. Clim.* 30 (2017) 5419–5454.
- [9] Gracia Amillo, A.M.; Taylor, N.; Martinez A.M.; Dunlop E.D.; Mavrogiorgios P.; Fahl F.; Arcaro G.; Pinedo I. 2021. “Adapting PVGIS to Trends in Climate, Technology and User Needs.” In *38th European Photovoltaic Solar Energy Conference and Exhibition (PVSEC)*, 907–11.
- [10] Grini, Sigbjørn. 2015. ‘Quality Control of Global Solar Irradiation Measured at Four Stations in Eastern Norway’.
- [11] C.A. Gueymard, Revised composite extraterrestrial spectrum based on recent solar irradiance observations, *Sol. Energy* 169 (2018) 434–440.
- [12] Y. Harada, H. Kamahori, C. Kobayashi, H. Endo, S. Kobayashi, Y. Ota, H. Onoda, K. Onogi, K. Miyaoka, K. Takahashi, ‘The JRA-55 reanalysis: representation of atmospheric circulation and climate variability’, *J. Meteorol. Soc. Japan Ser. II* 94 (2016) 269–302.
- [13] H. Hersbach, B. Bell, P. Berrisford, S. Hirahara, A. Horányi, J. Muñoz-Sabater, J. Nicolas, C. Peubey, R. Radu, D. Schepers, A. Simmons, C. Soci, S. Abdalla, X. Abellan, G. Balsamo, P. Bechtold, G. Biavati, J. Bidlot, M. Bonavita, G. De Chiara, P. Dahlgren, D. Dee, M. Diamantakis, R. Dragani, J. Flemming, R. Forbes, M. Fuentes, A. Geer, L. Haimberger, S. Healy, R.J. Hogan, E. Hölm, M. Janisková, S. Keeley, P. Laloyaux, P. Lopez, C. Lupu, G. Radnoti, P. de Rosnay, I. Rozum, F. Vamborg, S. Villaume, J.-N. Thépaut, The ERA5 global reanalysis, *Q. J. R. Meteorol. Soc.* 146 (2020) 1999–2049.
- [14] T.E. Hoff, R. Perez, J. Kleissl, D. Renne, J. Stein, Reporting of irradiance modeling relative prediction errors, *Prog. Photovolt. Res. Appl.* 21 (2013) 1514–11159.
- [15] G. Huang, Z. Li, X. Li, S. Liang, K. Yang, D. Wang, Y.i. Zhang, Estimating surface solar irradiance from satellites: Past, present, and future perspectives, *Remote Sens. Environ.* 233 (2019) 111371.
- [16] IEA PVPS. 2023. “Snapshot of Global PV Markets.” In.
- [17] P. Ineichen, R. Perez, A new airmass independent formulation for the Linke turbidity coefficient, *Sol. Energy* 73 (2002) 151–1117.
- [18] P.A. Jiménez, J. Yang, J.-H. Kim, M. Sengupta, J. Dudhia, Assessing the WRF-solar model performance using satellite-derived irradiance from the national solar radiation database, *J. Appl. Meteorol. Climatol.* 61 (2022) 129–142.
- [19] M. Journée, C. Bertrand, Quality control of solar radiation data within the RMIB solar measurements network, *Sol. Energy* 85 (2011) 72–86.
- [20] V. Kallio-Myers, A. Riihelä, P. Lahtinen, A. Lindfors, Global horizontal irradiance forecast for Finland based on geostationary weather satellite data, *Sol. Energy* 198 (2020) 68–80.
- [21] S. Kobayashi, Y. Ota, Y. Harada, A. Ebata, M. Moriya, H. Onoda, K. Onogi, H. Kamahori, C. Kobayashi, H. Endo, K. Miyaoka, K. Takahashi, ‘The JRA-55 Reanalysis: general specifications and basic characteristics’, *J. Meteorol. Soc. Japan Ser. II* 93 (2015) 5–48.
- [22] M. Lefèvre, A. Oumbe, P. Blanc, B. Espinar, B. Gschwind, Z. Qu, L. Wald, M. Schroedter-Homscheidt, C. Hoyer-Klick, A. Arola, A. Benedetti, J.W. Kaiser, J. Morcrette, McClear: a new model estimating downwelling solar radiation at ground level in clear-sky conditions, *Atmos. Meas. Tech.* 6 (2013) 2403–2418.
- [23] Moser, D., S. Lindig, M. Herz, B. Müller, I. Horvath, A. Schils, S. Ramesh, M. Green, J. Vedde, D. Barnard, B. Herteleer, J. A. Tsanakas, J. Ascencio-Vasquez, and M. Richter. 2020. “Benchmarking Yield Assessment Exercise in Different Climates within an International Collaboration Framework.” In *37th European Photovoltaic Solar Energy Conference and Exhibition*, 1317–23.
- [24] NVE. ‘senorge.no’, Accessed 15.07.2021.
- [25] D. Palmer, E. Koubli, I. Cole, T. Betts, R. Gottschalg, Satellite or ground-based measurements for production of site specific hourly irradiance data: Which is most accurate and where? *Sol. Energy* 165 (2018) 240–255.
- [26] R. Perez, P. Ineichen, K. Moore, M. Kmiecik, C. Chain, R. George, F. Vignola, A new operational model for satellite-derived irradiances: description and validation, *Sol. Energy* 73 (2002) 307–317.
- [27] U. Pfeifroth, A. Sanchez-Lorenzo, V. Manara, J. Trentmann, R. Hollmann, Trends and variability of surface solar radiation in Europe based on surface- and satellite-based data records, *J. Geophys. Res. Atmos.* 123 (2018) 1735–1754.
- [28] Z. Qu, A. Oumbe, P. Blanc, B. Espinar, G. Gesell, B. Gschwind, L. Klüser, M. Lefèvre, L. Saboret, M. Schroedter-Homscheidt, L. Wald, Fast radiative transfer parameterisation for assessing the surface solar irradiance: The Heliosat-4 method, *Meteorol. Z.* 26 (2017) 33–57.
- [29] M. Schroedter-Homscheidt, F. Azam, J. Betcke, N. Hanrieder, M. Lefèvre, L. Saboret, Y.-M. Saint-Drenan, Surface solar irradiation retrieval from MSG/SEVIRI based on APOLLO Next Generation and HELIOSAT-4 methods, *Meteorol. Z.* 31 (2022) 455–476.
- [30] C. Thomas, E. Wey, P. Blanc, L. Wald, M. Lefèvre, Validation of HelioClim-3 Version 4, HelioClim-3 Version 5 and MACC-RAD Using 14 BSRN Stations, *Energy Procedia* 91 (2016) 1059–1069.
- [31] R. Urraca, A.M. Gracia-Amillo, E. Koubli, T. Huld, J. Trentmann, A. Riihelä, A. V. Lindfors, D. Palmer, R. Gottschalg, F. Antonanzas-Torres, Extensive validation of CM SAF surface radiation products over Europe, *Remote Sens. Environ.* 199 (2017) 171–186.
- [32] R. Urraca, T. Huld, A. Gracia-Amillo, F.J. Martinez-de-Pison, F. Kaspar, A. Sanz-Garcia, Evaluation of global horizontal irradiance estimates from ERA5 and COSMO-REA6 reanalyses using ground and satellite-based data, *Sol. Energy* 164 (2018) 339–354.
- [33] L. Vuilleumier, M. Hauser, C. Félix, F. Vignola, P. Blanc, A. Kazantzidis, B. Calpini, Accuracy of ground surface broadband shortwave radiation monitoring, *J. Geophys. Res. Atmos.* 119 (2014), 13,838–13,60.
- [34] D. Yang, Kriging for NSRDB PSM version 3 satellite-derived solar irradiance, *Sol. Energy* 171 (2018) 876–883.
- [35] D. Yang, J.M. Bright, Worldwide validation of 8 satellite-derived and reanalysis solar radiation products: a preliminary evaluation and overall metrics for hourly data over 27 years, *Sol. Energy* 210 (2020) 3–19.